AIAA JOURNAL
Vol. 46, No. 7, July 2008

Stability and Performance of a Smart Double Panel with Decentralized Active Dampers

Neven Alujević,* Kenneth D. Frampton,† and Paolo Gardonio‡
University of Southampton,
Southampton, England, SO17 1BJ, United Kingdom

DOI: 10.2514/1.34572

This paper presents a theoretical study of active control of sound transmission through a double panel using decentralized active dampers acting between the two panels. The double panel consists of a thin aluminum plate (the source panel) and a polymer honeycomb plate (the radiating panel), coupled structurally by elastic mounts and coupled acoustically by the air confined in a shallow cavity between the plates. The control forces are applied using a 4 × 4 regular array of actuators located in the cavity, which can react between the two plates. Each actuator end is equipped with a velocity sensor. The two junction-velocity signals are weighted and combined into error signals. By varying the weighting factor, a variety of error signals can be created. The impact of the weighting factor on the performance of the control and the stability of the feedback loops is investigated. It was found that the range of weighting factors for which the feedback loops are unconditionally stable is limited, and the performance of the active control depends upon the weighting factor used.

Nomenclature

c_{air}	=	speed of sound in air
E_m	=	Young's modulus of the elastic mounts
E_r	=	Young's modulus of the radiating panel
E_s	=	Young's modulus of the source panel
f_c	=	control force
f_{rc}	=	radiating-panel component of the control force
f_{sc}	=	source-panel component of the control force
h_m	=	height of the elastic mounts
h_r	=	thickness of the radiating panel
h_s	=	thickness of the source panel
l_x	=	length of the panels
l_y	=	width of the panels
$T_{cc}^{r,r}$	=	point mobility of the radiating panel
$T_{cc}^{r,s}$	=	transfer mobility, source to radiating
$T_{cc}^{s,r}$	=	transfer mobility, radiating to source
$T_{cc}^{s,s}$	=	point mobility of the source panel
v_E	=	error velocity
v_{rc}	=	radiating-panel velocity at a control location
v_{sc}	=	source-panel velocity at a control location
α	=	velocity weighting factor
α_{crit}	=	critical-velocity weighting factor
δ_o	=	largest negative real part of sensor-actuator frequency response function
ζ_c	=	modal damping ratio of the air cavity
η_m	=	elastic-mount loss factor
η_r	=	radiating-panel loss factor
η_s	=	source-panel loss factor
ρ_{air}	=	air mass density
ρ_r	=	radiating-panel mass density
ρ_s	=	source-panel mass density
ϕ_m	=	diameter of the elastic mounts

Received 13 September 2007; revision received 27 February 2008; accepted for publication 5 March 2008.

*Research Student, Institute of Sound and Vibration Research.
†Senior Lecturer, Institute of Sound and Vibration Research.
‡Professor of Systems Dynamics and Control, Institute of Sound and Vibration Research.

I. Introduction

AIRCRAFT cabin noise is mainly due to exterior broadband random disturbances such as engine noise or turbulent boundary-layer noise [1]. A great deal of research has therefore been dedicated to the sound transmission through aircraft fuselage sections. Fuselage-noise-transmission research has mainly progressed in two directions: either large-scale realistic simulations such as finite element models or simplified models consisting of two flat plates that are coupled acoustically only. In the latter case, simple analytical expressions can be derived that give better physical insight into the fundamental phenomena governing sound transmission [2].

It has been found that double panels are good noise insulators at frequencies higher than the characteristic mass–air–mass resonance, but the low-frequency sound-transmission ratio remains relatively high [2]. This problem is commonly solved by placing heavy damping materials into the cavity between the two plates, although such treatment tends to increase the weight of the structure [3–6]. A more recent solution to the problem is the use of active control and, more specifically, active damping.

Direct-velocity feedback loops applied on plate structures produce the active damping effect, which tends to reduce the response and sound transmission at the resonant frequencies of the plate [7–10]. This control mechanism can also be effectively used to control the response and sound radiation of double-panel structures, which are characterized at low frequencies by well-separated resonances that involve lightly damped vibrations of the structurally and acoustically coupled panels [11]. To guarantee unconditional stability of a direct feedback control loop, sensor and actuators should be dual and collocated [12–15]. During the past 15 years, much research work has been carried out to develop realistic sensor-actuator transducers for smart structures [12], which behave as dual and collocated pairs. Yet, with real systems, the complexity of the actuation and sensing mechanisms always leads to the conditional stability of the feedback loops [16–22]. Consequently, only limited feedback gains can be implemented, which may not be sufficient to produce acceptable active damping effects for the particular problem.

For example, Gardonio et al. [16–18] studied a decentralized velocity feedback control system with square piezoelectric patch actuators and inertial accelerometer sensors located at the patch centers, for the vibration control of a rectangular plate. With this arrangement, good active damping effects have been achieved up to 1 kHz [16–18]. However, the maximum feedback gains that could be implemented were limited, due to the stability problems. This is because such sensors and actuators behave as dual and collocated

pairs only at lower frequencies, at which the plate bending wavelength is larger than the principal piezoelectric patch dimensions [12,16–18]. Alternatively, a decentralized velocity feedback control system with proof-mass electrodynamic actuators and collocated accelerometer sensors has been investigated for the vibration control of a plate [20,22]. Also in this case, only a limited range of feedback gains could be implemented, because the fundamental resonances of the actuators tend to destabilize the feedback control loops [22].

This study deals with active control of the low-frequency sound transmission through a simplified model of an aircraft double panel. A multi-input/multi-output (MIMO) decentralized velocity feedback control system is considered, which potentially can offer reductions of broadband noise without the complexity of fully coupled MIMO systems [7–10]. In this paper, an alternative actuating scheme is considered for the development of a smart double panel using multiple independent force/velocity feedback control loops. Electrodynamic actuators placed in the air cavity between the two plates are used, which react from either plate so that they can develop a bending force between the two plates. Two velocity sensors are attached to either end of each actuator. Using this configuration permits the creation of the relative velocity between the two plates. This relative velocity is dual, with the reactive force actuator resulting in a potentially unconditionally stable control system. Previous work has indicated that good control can be achieved using such decentralized relative-velocity feedback control loops [11]. To improve the control performance, a specially configured error signal is considered in this paper that independently weights the two measured velocities. Thus, the principal contribution of the work presented here is the investigation of the feedback-loop stability and the corresponding control performance with respect to these weights.

The paper is structured into four sections. Section II describes the double-panel system and the mathematical model used for the study. Section III discusses the implementation of the decentralized control system and the analysis of the performance. Section IV gives a detailed analysis of the stability of the feedback loops with respect to the weighting factors used. A sensitivity study is also performed, which investigates the dependence of the critical weighting factor required to guarantee unconditional stability with reference to the physical properties of the double panel.

II. Model Problem

As shown in Fig. 1, the system considered in this study consists of two panels that are structurally and acoustically coupled via elastic mounts and the air in the cavity between the panels, respectively.

The source panel is excited by an acoustic plane wave, and the radiating panel radiates sound into a free field. The source panel is assumed to be simply supported along the four edges. It is modeled as a $414 \times 314 \times 1$ mm aluminum panel, which represents a section of the outer skin of a typical passenger aircraft. To excite all the vibration modes of the source panel, the acoustic plane wave excitation has azimuthal and elevation angles of 45 and 45 deg, respectively. The radiating panel is modeled as a plate with free boundary conditions along the four edges, although structurally connected to the source panel by means of four rubber mounts. The radiating panel has the same x and y dimensions as the source panel, but it is made of a honeycomb polymer material with 3-mm thickness. These properties were chosen to emulate a typical aircraft trim panel. The physical properties of the modeled double-panel configuration are summarized in Table 1.

As shown in Fig. 1, the double panel is equipped with a 4×4 array of reactive point-force actuators located in the air cavity between the two plates and collocated velocity sensors placed on either panel, which can be used to generate direct-velocity feedback loops. The 4×4 array of sensors and actuators were equally spaced along the x and y directions.

The mathematical model used for this study assumes that the system is divided into three elements: the source panel, the radiating panel, and the structure-borne and airborne transmission paths. The structure-borne transmission path gives the sound transmission via the elastic mounts, and the airborne path gives the sound transmission via the air confined between the radiating and the source panels. The response of each of these elements is evaluated using point and transfer mobility or impedance functions. The air coupling of the panels is calculated using transfer impedances between a finite number of elements on the surface of the panels. The excitation of the source panel by the incident acoustic wave and the radiated sound power from the radiating panel are also calculated by assuming that two panels are divided into the same number of elements. This number is obtained by choosing element dimensions to be $l_{x,e} = l_x/(4M)$ and $l_{y,e} = l_y/(4N)$, where M and N are higher structural modal orders used in calculations. The coupling via the elastic mounts is modeled as viscoelastic out-of-plane force so that point impedances can be used to model this coupling at the mount locations. A detailed description of the fully coupled vibroacoustic model used in this study can be found in [4,11,23] and its validation against other modeling techniques can be found in [5].

III. Implementation of the Velocity Feedback Control

A. Error-Signal Configuration for the Reactive Actuators

Previous research carried out by the authors has shown that a control technique using reactive actuators driven by relative-velocity error signals in double panels offers promising reductions of the radiating plate kinetic energy and the sound transmission [11]. The reductions were, however, much less than the reductions obtained using idealized skyhook actuators acting on the radiating plate [11]. To improve the performance of the MIMO direct-velocity feedback loops using the reactive actuation scheme, the error signal v_E is formed as the sum of the weighted velocities v_{rc} and v_{sc} measured at the two actuation locations:

$$v_E = v_{\mathrm{rc}}(1-\alpha) - v_{\mathrm{sc}}\alpha \tag{1}$$

If $\alpha = 0$, the error signals are formed purely from the radiating-panel junction velocities at the control locations. In contrast, if $\alpha = 1$,

Table 1 Physical properties of the double-panel system

	Source panel			*Radiating panel*	
Length	l_x	0.414 m	Length	l_x	0.414 m
Width	l_y	0.314 m	Width	l_y	0.314 m
Thickness	h_s	0.001 m	Thickness	h_s	0.003 m
Mass density	ρ_s	2720 kg/m^3	Mass density	ρ_r	255 kg/m^3
Young's modulus	E_s	71×10^{10} N/m^2	Young's modulus	E_r	15×10^{10} Pa
Poisson's ratio	ν_s	0.33	Poisson's ratio	ν_r	0.3
Loss factor	η_s	0.01	Loss factor	η_r	0.03
	Elastic mounts			*Air cavity*	
Diameter	ϕ_m	0.01 m	Length	l_x	0.414 m
Height	h_m	0.03 m	Width	l_y	0.314 m
Position x	x_m/l_x	5%, 95%	Depth	h_c	0.03 m
Position y	y_m/l_y	5%, 95%	Air density	ρ_{air}	1.19 kg/m^3
Young's modulus	E_m	1.5×10^6 Pa	Speed of sound	c_{air}	343 m/s
Loss factor	η_m	0.05	Modal damping ratio	ζ_c	0.05

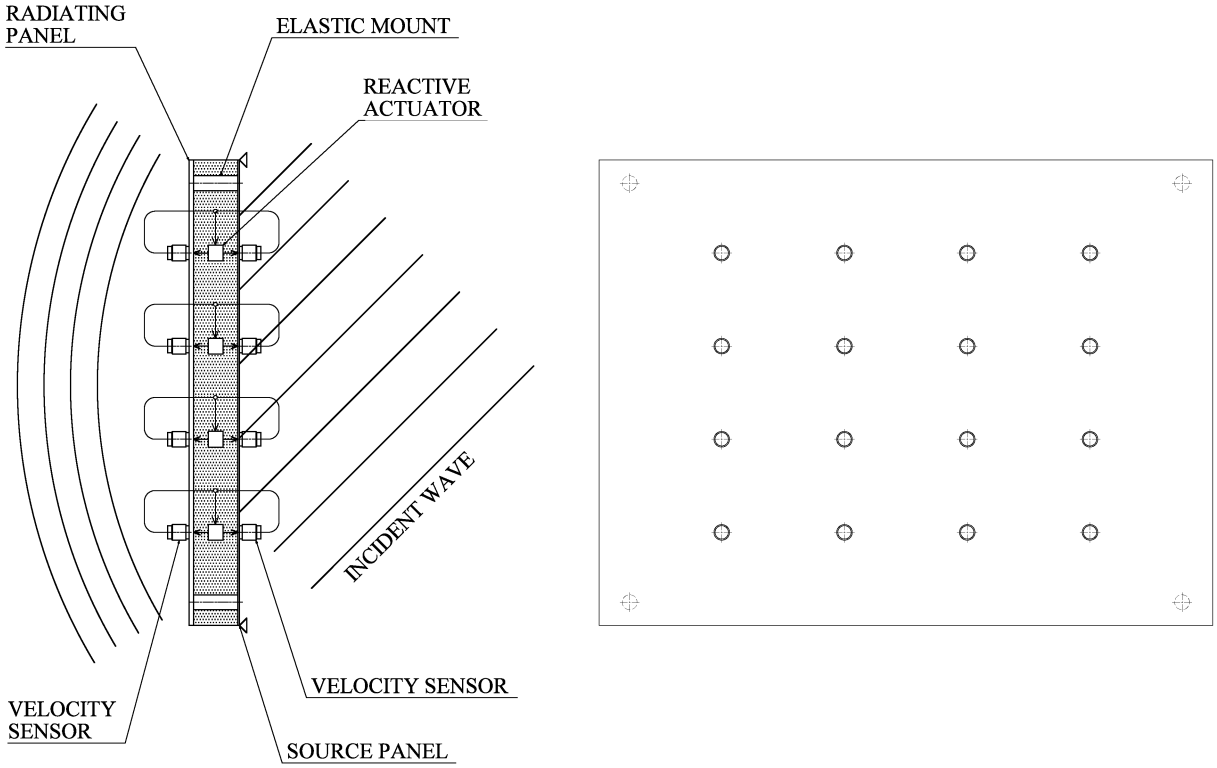

Fig. 1 Smart double panel with reactive force actuators and collocated velocity sensors.

the error signals are formed purely from the source-panel junction velocities. If $\alpha = 0.5$, the error signals are then proportional to the relative velocity of the two actuator junctions at the control locations. This relative error velocity is dual and collocated to the reactive actuation force, which guarantees unconditional stability of the feedback loop, as long as the dynamics of real sensors and actuators are negligible. By changing the weighting factor from zero to one, it is possible to continuously transform the error signal from pure radiating-panel velocity toward pure source-panel velocity. The technique of forming the error signal and some consequences of its use are now discussed in more detail.

A single actuator produces a reactive force designated as f_c (control force) which, as shown in Fig. 2, is applied to the radiating panel ($f_{\mathrm{rc}} = f_c$) and to the source panel ($f_{\mathrm{sc}} = -f_c$). Because of the acoustical/structural coupling of the panels, each of the control force components f_{rc} and f_{sc} contributes to the motion of each panel at the source and radiating actuator junctions. For example, the radiating-panel control force component f_{rc} contributes to the radiating-panel velocity v_{rc} at the radiating-panel sensor location via the corresponding point mobility function $T_{cc}^{r,r}(\omega)$ of the coupled system, but it also contributes to the source-panel velocity v_{sc}at the source-panel sensor location via the corresponding transfer mobility function $T_{cc}^{r,s}(\omega)$ of the coupled system (Fig. 2). On the other hand, the source-panel secondary force component f_{sc} contributes to the source-panel velocity v_{sc} at the source sensor location via the corresponding point mobility function $T_{cc}^{s,s}(\omega)$ of the coupled system, but it also contributes to the radiating-panel velocity v_{rc} at the sensor location via the corresponding transfer mobility function $T_{cc}^{s,r}(\omega)$ of the coupled system (Fig. 2). Therefore, the use of the reactive actuation scheme includes indirect-actuation paths, which occur through structural and acoustical coupling of the two plates. The existence of the indirect-actuation paths can affect the stability of the feedback loops if the α factor is different from 0.5, in which case the effects of the two indirect-actuation paths cancel out.

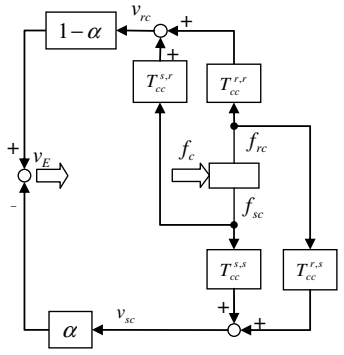

Fig. 2 Configuration of the error signal.

Emphasizing a velocity signal measured either at the source or the radiating junction of an actuator may improve the performance of the active control in comparison with the case of pure relative damping with $\alpha = 0.5$. Therefore, in the next subsection, performance of the decentralized control system is analyzed with reference to velocity weighting factors that range from 0 to 1.

B. Control Performance

The performance of the MIMO decentralized control is analyzed with reference to the spatially averaged kinetic energy of the radiating panel and the sound-transmission ratio [7], in the frequency range from 10 to 3 kHz. The reduction of the radiating plate kinetic energy can be used to estimate the reductions of the near-field sound levels due to the active control. On the other hand, the sound-transmission ratio reflects the reductions of the sound levels in the far field [7].

The plots in Fig. 3 show the mean kinetic energy of the radiating panel and sound-transmission ratio when the 16 feedback loops are implemented with a $\alpha = 0.375$ weighting factor, which emphasizes the radiating-panel velocity and, as shown in Sec. IV, guarantees unconditional stability.

The solid lines in the two plots of Fig. 3 represent either the sound-transmission ratio or kinetic energy of the panels without control. At frequencies below the first acoustic resonance in the cavity at 414 Hz and below the mass–air–mass resonance of the double panel at about 440 Hz, the response and sound radiation are characterized by well-separated resonances that are due to the coupled response of the two panels via the four mounts and the air in the cavity, which acts as an additional distributed spring. The plot with the kinetic energy is characterized by a larger number of resonances than that of the

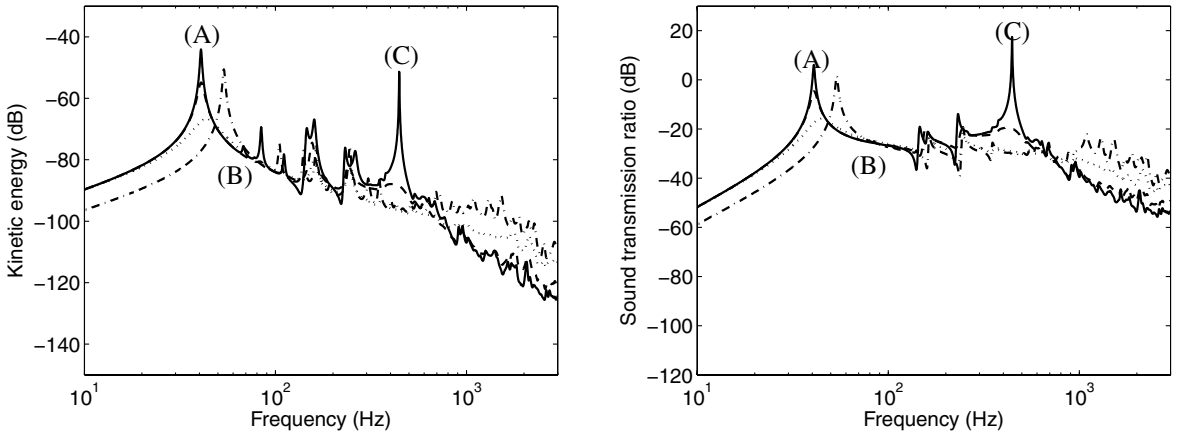

Fig. 3 Direct-velocity feedback using reactive control actuators with velocity weighting factor equal to $\alpha = 0.375$: case without control (solid lines), small feedback gains (dashed lines), optimal feedback gains (dotted lines), and excessive feedback gains (dashed-dotted lines).

sound-transmission ratio. This is due to two phenomena: First, the modes of the radiating panel with small volumetric components have very small sound-radiation efficiency. Second, the acoustic coupling between modes of the two panels with small volumetric components is relatively weak. Therefore, the resonance peaks associated to nonvolumetric modes (i.e., even–even or even–odd modes) of either source or radiating panels have little amplitudes, which can hardly be distinguished in the spectrum in some cases (see, for example, resonances specified by letter B in Fig. 3).

At frequencies above 440 Hz, the sound-transmission ratio is characterized by an initial 18 dB per octave roll-off, which is typical for double panels above their mass–air–mass resonance [2]. The modal density at those high frequencies is much larger, because, together with the modes controlled by the two plates, there are also modes controlled by the cavity. Thus, the rising modal overlap effect smoothes out the spectra of the response and the sound radiation, which no longer show well-separated lightly damped resonance peaks.

When the 16 feedback control gains are turned up, active damping action is produced so that (as shown by dashed and dotted lines in Fig. 3) the response of the radiating panel (and thus the sound radiation) tends to descend at the radiating-panel low-order-mode resonant frequencies. If very large gains are applied, as shown by dashed-dotted lines, the response of the radiating panel is characterized by a new set of modes. These modes are defined by the control forces that cause the two panels to move together as if they were connected by very rigid fasteners, because the α value is quite close to 0.5 (relative damping). Thus, new sets of resonances are produced at slightly higher frequencies that have relatively higher amplitudes. In other words, the double panel tends to become a sort of thick and light single panel with a higher stiffness-mass ratio. The response is then again characterized by lightly damped resonances, because having the control positions of the source and the radiating panel connected by the rigid links prevents the generation of active damping. The new resonances occur at higher frequencies; for example, the lowest resonant frequency of 39 Hz shifts to 54 Hz. The sound-transmission ratio at frequencies above the mass–air–mass resonance and with large feedback gain rolls off with a rate of 12 dB per octave. This roll-off is a characteristic of single panels rather than double panels [2].

Figure 4 illustrates the deflection shapes of the panel at three resonant frequencies for three different feedback-gain values. The top row of the plot shows the open-loop case, the center row illustrates the case when the 16 control units implement the control gains that give the largest active damping effect, as described later, and the bottom row depicts the deflection shapes when excessive control gains are applied so that the two panels are effectively linked together at the 16 control positions.

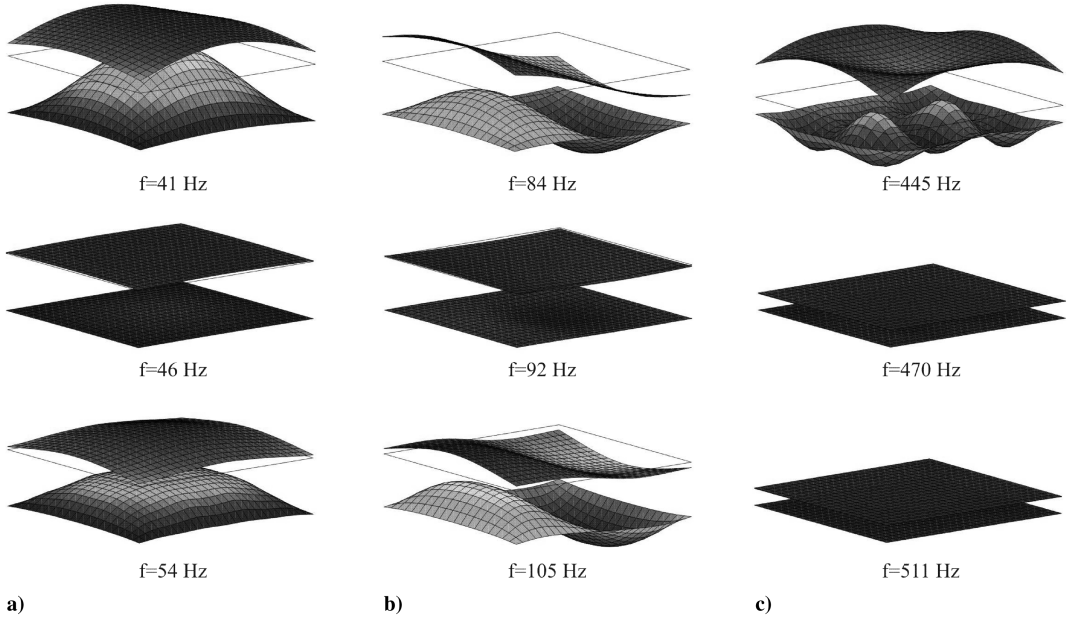

Fig. 4 Scaled deflection shapes of the two panels at the 1st (left column), 5th (center column), and 23rd (right column) resonances of the system, depicting deflection shapes with no control (top row), moderate gains (center row), very large feedback gains of $\alpha = 0.375$ (bottom row).

The deflection shape designated by A in Fig. 4 is characterized by a (1, 1) volumetric mode of the source panel, which induces an even rigid-body mode of the resiliently mounted radiating panel (the first mode of the double panel). The four flexible mounts change the vibration field of the radiating panel in such a way that it looks like a (1, 1) flexible mode that is pinned at the four mounting points. The mode shape designated by B in Fig. 4 is characterized by a (2, 1) mode of the source panel, which induces a rocking rigid-body mode of the resiliently mounted radiating panel. In this case, the four mounts constrain the vibration of the radiating panel at the corners. Finally, the deflection shape C in Fig. 4 (mass–air–mass), in addition to the air acting like a spring between two masses, is characterized by a strong coupling between the two panels via the first cavity mode (1, 0, 0) that resonates. As a result, the responses of the two panels are influenced by the cavity mode that induces a cosinusoidal field in the x direction on the source panel. At the mass–air–mass resonance, the 16 control units efficiently prevent the excitation of the resonant cavity mode, and the relative out-of-phase motion of the two plates. Thus, when the control gains are raised, the response of the two panels monotonically falls off, even for excessive control gains (Fig. 4, column C, at the bottom).

The two plots in Fig. 5 show kinetic energy of the radiating panel and the sound-transmission ratio normalized with respect to the open-loop case, integrated from 0 to 3 kHz, and plotted against the feedback gain. The curves in each plot were derived by varying the sensor weighting factor α between 0.875 and 0.375, where $\alpha = 0.375$ is the smallest value of α for which the feedback loop is unconditionally stable. The dashed-dotted curves in Fig. 5 represent the reductions that can be generated by a decentralized MIMO feedback system that uses ideal skyhook actuators and velocity sensors located on the radiating panel [11].

The results shown in Fig. 5 indicate that the skyhook actuation is, by far, the best arrangement. The response and sound-radiation reductions are twice as big as those obtained with the best reactive force-feedback configuration. However, in practice, it is normally necessary to have a reactive arrangement to obtain a pure force actuation. This could be obtained by reacting against a suspended mass, but in such cases, the feedback loop is only conditionally stable [20,22] and does not permit the implementation of the control gains large enough to equal the control effects predicted for skyhook actuation.

When the reactive control scheme is used, the kinetic energy of the radiating panel and the sound-transmission ratio monotonically decrease as the 16 control gains are raised from zero to approximately 10–100 Ns/m and for all values of α. When the smallest velocity weighting factor is used ($\alpha = 0.375$), the maximum reduction in kinetic energy is about 16 dB and the maximum reduction in the sound-transmission ratio is about 25 dB. When the control gain is increased beyond the point of maximum attenuation, the reduction in kinetic energy and sound-transmission ratio degrades because the control system tends to connect the panels at the control positions; this effect prevents active damping and introduces a modal response characterized by new lightly damped resonances.

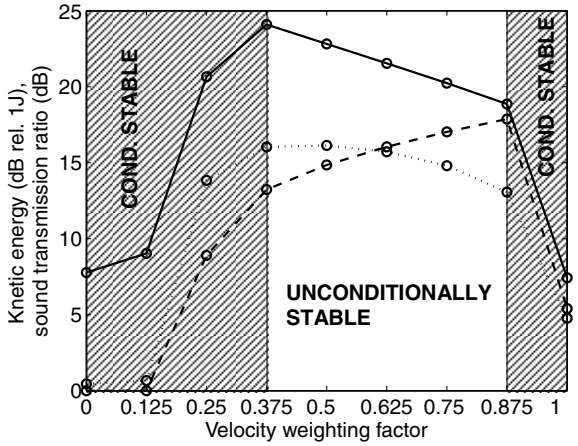

Fig. 6 Maximum reductions of the a) sound-transmission ratio (solid line), b) normalized total kinetic energy of the source panel (dashed line), and c) normalized total kinetic energy of the radiating panel (dotted line).

The solid and dotted lines in Fig. 6 show that the best reductions of sound-transmission ratio and kinetic energy of the radiating panel are obtained when α is approximately 0.375. This corresponds to error signals that are tuned in such a way as to weight the radiating-panel velocities more than the source-panel velocity. In contrast, as shown by the dashed line, the best reduction of source-panel kinetic energy is obtained when α is approximately 0.875. In this case, the error signals are tuned in such a way as to weight the source-panel velocities more. Also shown in Fig. 6 are the ranges of the velocity weighting factor α for which the feedback loop is conditionally and unconditionally stable. This influence of the velocity weighting factor is of critical importance to the stability, as demonstrated in the following section.

IV. Stability

A. Sensor-Actuator Open-Loop Frequency Response Function

As mentioned before, indirect-actuation paths can cause stability problems if reactive actuators are combined with unbalanced relative-velocity sensors on the double-panel system considered. In this study, the Nyquist criterion is used to assess the stability of a single control loop. Strictly, the stability of all 16 control loops should be assessed with a generalized form of the Nyquist criterion

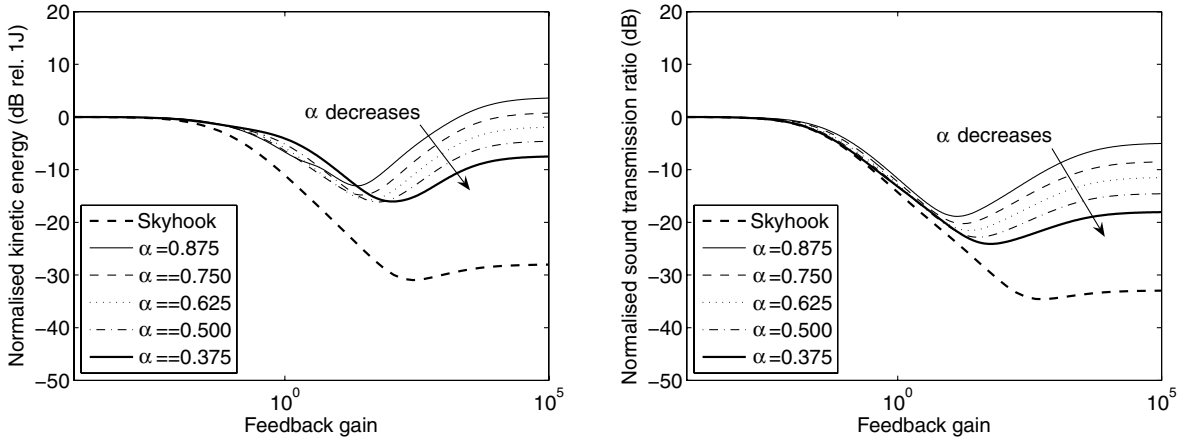

Fig. 5 Normalized kinetic energy of the radiating panel (left) and sound-transmission ratio (right), integrated from 0 to 3 kHz, plotted against the control gain for the different α factor values: $\alpha = 0.875$ (solid faint line), $\alpha = 0.75$ (dashed faint line), $\alpha = 0.625$ (dotted faint line), $\alpha = 0.5$ (dashed-dotted faint line), and $\alpha = 0.375$ (solid line), and for a decentralized MIMO feedback system that uses 16 ideal skyhook actuators and velocity sensors on the radiating panel (dashed line).

[8,9,24]. However, the stability analysis of a single control unit can be better interpreted in terms of the physics of the system. Moreover, any instability of a single unit is likely to affect the stability of the 16-channel control system. Thus, the stability of a single control unit is assumed here as a necessary condition for the stability of the whole 16-channel control system.

Figure 7a shows the Bode (left) and Nyquist (right) plots of the sensor-actuator open-loop frequency response function (FRF), assuming a velocity weighting factor $\alpha = 0.5$. The plots are derived considering one of the inner four units of the actuator/sensor array. Note that the FRF phase is confined between ± 90 deg; thus, there is no negative real part in the Nyquist plot and the feedback loop is bound to be unconditionally stable. One might expect intuitively that the case of $\alpha = 0.5$ would be unconditionally stable because the reactive control force is proportional to the opposite of the relative velocity of the panels and thus produces relative damping. A decrease in the FRF amplitude with increase in frequency is noticeable, which suggests that the control performance at higher frequencies is bound to decrease.

Further simulations have shown that the feedback loop continues to be unconditionally stable for values of α down to 0.375. If the velocity weighting factor is further decreased below 0.375, then the loop will be conditionally stable. This is demonstrated in Fig. 7b, which shows the FRF and Nyquist plots for $\alpha = 0.1$. The largest negative real part of the FRF is indicated in the Nyquist plot by δ_o. According to the Nyquist criterion, if $\delta_o = 0$, then the loop is unconditionally stable. In contrast, if $\delta_o < -1$, then the feedback loop is unstable. Finally, if $-1 < \delta_o < 0$, then the loop is conditionally stable, although control-spillover effects are likely to occur at the frequencies at which the locus enters the circle of unit radius centered at $-1 + 0j$. Because δ_o equals 0.4 for the control unit in consideration, the condition under which stability can be guaranteed is that the feedback gain must be less than 2.5 Ns/m. With the phase diagram, a 180-deg phase lag at approximately 40 Hz and another 180-deg phase lag at 84 Hz are noticeable. These phase lags occur at the resonant frequencies of the first and fifth modes of the double panel. The corresponding modes are characterized by the radiating panel being forced to follow the source-panel motion via the acoustical coupling (see Figs. 4a and 4b). To illustrate the importance of the acoustical indirect-actuation path, a simulation was performed that neglects the acoustical coupling of the two panels. The resulting FRF and Nyquist plot are depicted by the dashed lines in Fig. 7b. The feedback loop in that case would be unconditionally stable, because the phase of the open-loop FRF is constrained between ± 90 deg and thus the locus stays in the two positive real quadrants [23].

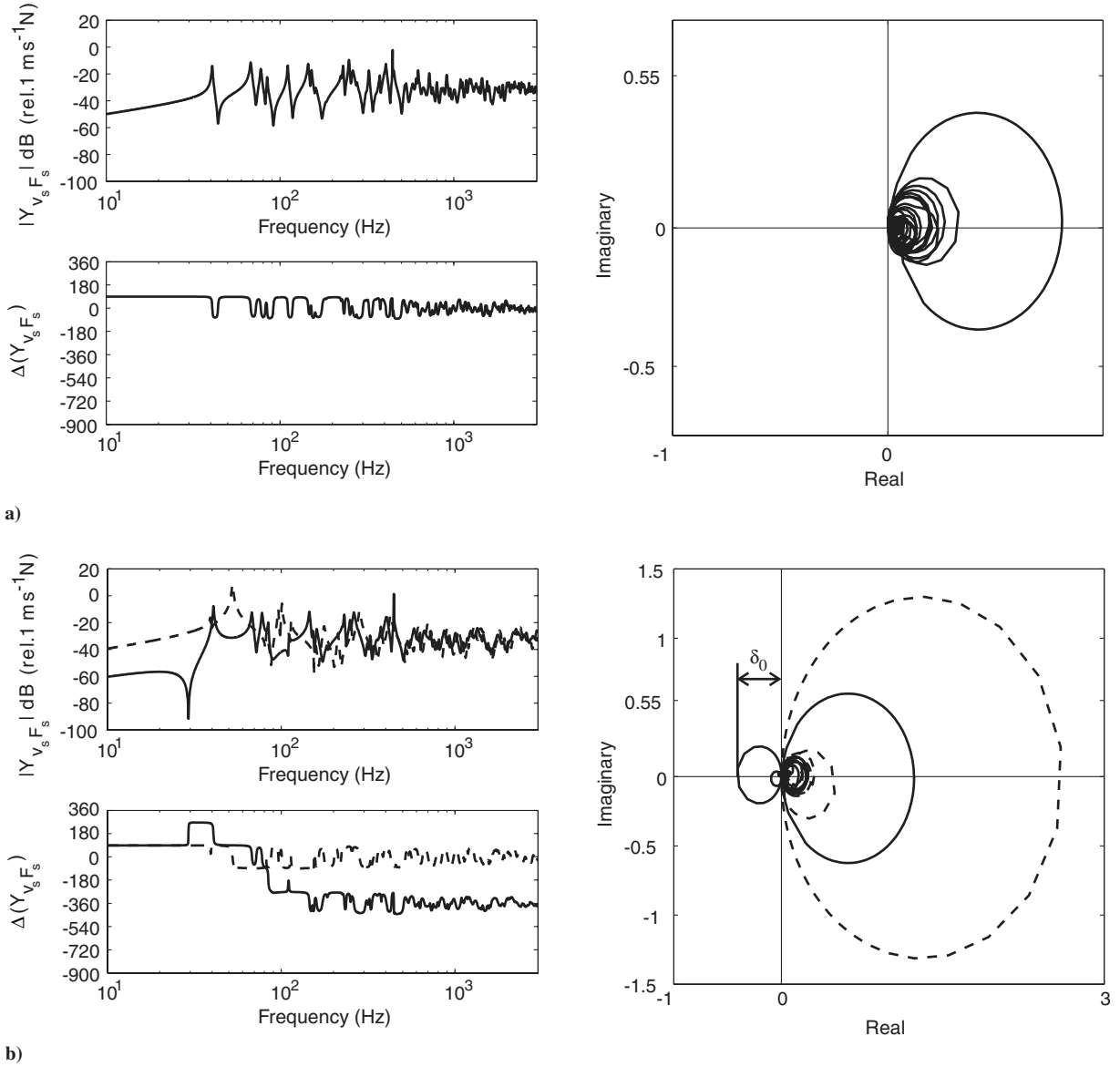

Fig. 7 Bode (left) and Nyquist (right) plots of the sensor-actuator FRF: A) for the velocity weighting factor of $\alpha = 0.5$, and B) for the velocity weighting factors of $\alpha = 0.1$ with (solid line) and without (dashed line) air coupling.

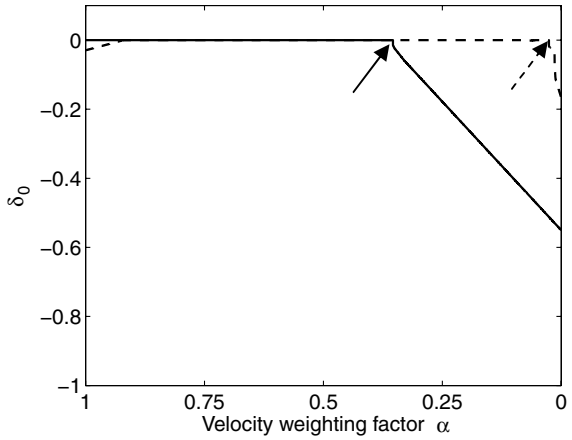

Fig. 8 The largest negative real part of the FRF, δ_0, plotted against the velocity weighting factor α when the acoustical coupling between the two panels is (solid line) or is not (dashed line) taken into account in the model.

B. Critical-Velocity Weighting Factor

Figure 8 shows the maximum value of δ_o (see Fig. 7a) plotted against the velocity weighting factor α for cases with and without acoustical coupling. It can be seen that acoustical coupling between the panels is the major cause of conditional stability for the control with the α factor lower than approximately 0.375. This value corresponds to the knee location in Fig. 8, as indicated by the solid arrow. Throughout this paper, the α factor of the knee, in which the feedback loop switches from conditional to unconditional stability, is considered to be the critical-velocity weighting factor α_{crit}. This is the weighting factor value that most emphasizes the radiating-panel velocities in the error signals while maintaining unconditional stability. Emphasizing the radiating-panel velocity in the error signals results in larger reductions of the sound-transmission ratio, as shown in Fig. 6. Therefore, in subsequent discussions, only velocity weighting values between 0 and 0.5 are considered to determine these critical factors α_{crit}.

Elastic mounts are another path for the indirect-actuation effect. Indeed, it is the coupling via the elastic mounts that limits the stability when the acoustical coupling is neglected (dashed line in Fig. 8). This coupling results in a critical-velocity weighing factor that is still bigger than zero, as shown by the dashed arrow in Fig. 8.

So far, the frequency response function considered was for one of the four inner control loops of the array (Fig. 1). However, the location of the feedback unit might also be an important factor in the stability. For example, the source panel is assumed to be simply supported along its edges. If a control unit is located exactly at an edge, then the velocity of the source panel at that point, v_{sc}, equals zero, as do the mobility functions $T_{cc}^{s,s}(\omega)$, $T_{cc}^{s,r}(\omega)$, and $T_{cc}^{r,s}(\omega)$ (see Fig. 2). Only the point mobility of the radiating-panel junction point $T_{cc}^{r,r}(\omega)$ is different from zero. Therefore, the indirect-actuation paths do not exist, and the error velocity due to control is purely determined by the radiating-panel control force component f_{rc}. As a consequence, even for $\alpha = 0$, control loops located at the edges should be unconditionally stable. This suggests that there must be spatial distribution of the critical-velocity weighting factor α_{crit}.

To verify this hypothesis, simulations were performed over a 34×34 grid of points evenly distributed over the surface of the double panel. The results are depicted in Fig. 9, which shows contour plots of α_{crit} over the panel's surface. Figure 9a indicates that the

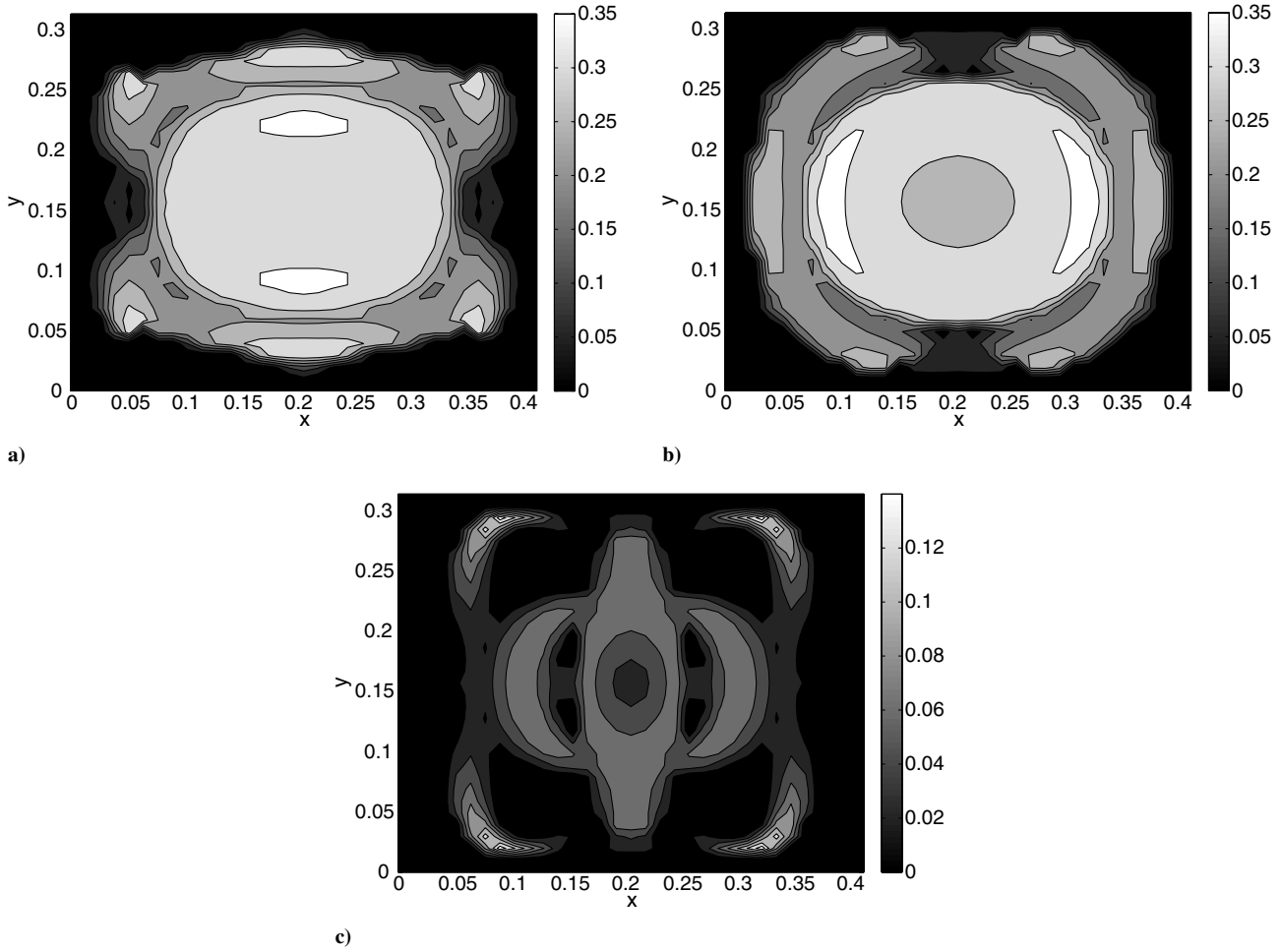

Fig. 9 Critical-velocity weighting factor distribution plotted over the surface of the double panel: a) fully coupled configuration, b) with neglected structural coupling, and c) with neglected acoustical coupling.

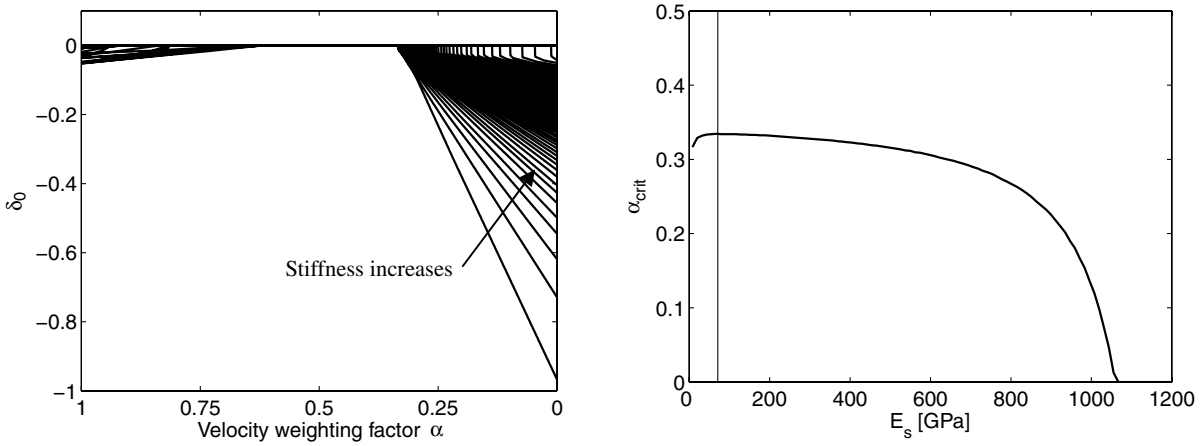

Fig. 10 Sensitivity of the critical-velocity weighting factor to the source-panel stiffness.

highest α factors to ensure unconditional stability are necessary near the center of the plate. As expected, zero values are found at the edges. Very high values can also be observed near the four corner mounts. If the mounts are removed, this effect vanishes, as shown in Fig. 9b. High values are still present in the center of the panel. Finally, if the air coupling is neglected, α_{crit} decreases significantly all over the panel, except in the vicinity of the mounts (Fig. 9c). This indicates that the acoustical coupling is the most important path for the indirect actuation when using reactive actuators in the double-panel model considered here.

C. Sensitivity Study

The value of the critical-velocity weighting factor varies from zero at the boundaries of the panel to 0.375 at the center of the panel. In other words, if the feedback loop is located near the simply supported edge of the source panel, then the source-panel velocity does not have to be included in the error signal. In contrast, if the control unit is to be located at the center of the panel, then the error signal has to include a large portion of the velocity at the source-panel junction to ensure unconditional stability and maximize the attenuation. However, the critical value of 0.375 at the center of the panel is strongly linked to the double-panel physical properties.

To investigate how α_{crit} depends upon physical properties of a double panel, an extensive sensitivity study has been performed [23]. The study considered variations of the following parameters: the source-panel stiffness and density, the radiating-panel stiffness and density, the stiffness of the structural mounts, the distance between the two plates, and the density of the cavity air.

The sensitivity study in [23] showed that the critical-velocity weighting factor is only slightly sensitive to the following parameters: the distance between the two plates, the stiffness and the density of the radiating panel, the stiffness of the mounting system, and the mass density of the source panel. A detailed study of these cases can be found in [23]. The parameters that significantly affect the critical-velocity weighting factor are the stiffness of the source panel and the density of the cavity air. If the source-panel stiffness is varied, then α_{crit} changes considerably, as shown in Fig. 10.

The left plot in Fig. 10 shows δ_0 plotted against the weighting factor. The location of the knee is shifted toward zero as the stiffness of the source-panel increases. In addition, if a weighting factor equal to zero is considered, the available gain margin increases as the stiffness of the source panel is increased (left plot). The right plot in Fig. 10, which explicitly depicts the dependence of α_{crit} upon the stiffness of the source plate, shows that the critical weighting factor decreases to zero as the source-panel stiffness increases. In fact, stiffening the source panel must lead to a decrease in the amplitude of the source-panel mobility functions. For example, in the extreme case of infinite stiffness of the source panel, it becomes a fixed reference base from which the actuators can react, and therefore the velocity measured by the source-panel junction sensor is equal to zero. Although the right plot shows that the critical-velocity weighting factor can be reduced to zero by increasing the stiffness of the source panel, it is worth noting that a relatively large increase in the stiffness is required. A similar effect is obtained if the density of the cavity air is reduced. Figure 11 shows the effect, following the same layout as in Fig. 10.

As the air density decreases, α_{crit} decreases. When the cavity-air density is zero, α_{crit} is still different from zero, due to the remaining structural coupling of the elastic mounts. Nevertheless, it is clear that reducing the density of the cavity air weakens the acoustical coupling path, which leads to an amplitude decrease of the transfer mobilities $T_{cc}^{s,r}(\omega)$ and $T_{cc}^{r,s}(\omega)$ that model the indirect-actuation paths.

The cavity air couples the two panels strongly. For example, the low-order deflection shapes A and B shown in Fig. 4 suggest that volumetric changes of the cavity air are very small, if not negligible. Because of that, any low-frequency motion of the source panel is

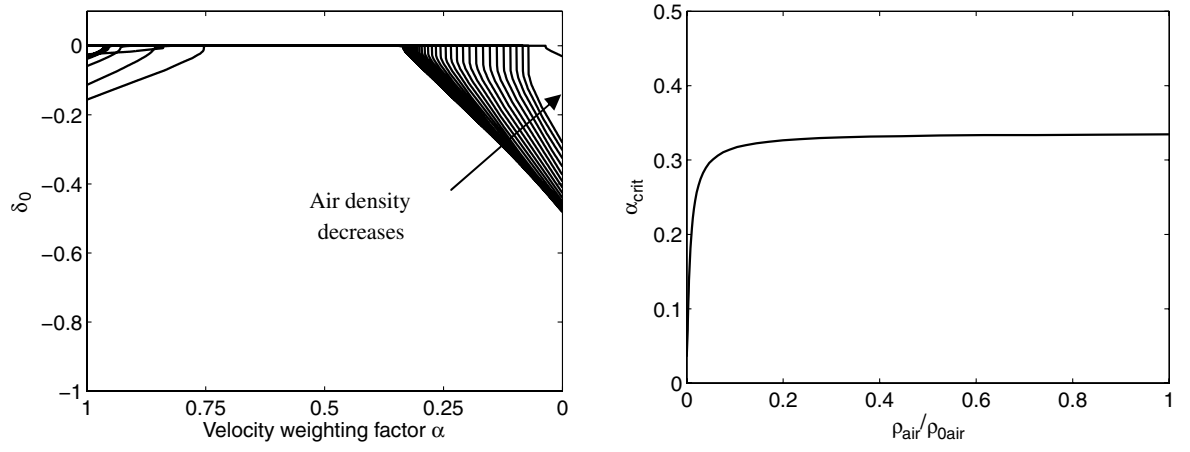

Fig. 11 Sensitivity of the critical-velocity weighting factor to the cavity-air density.

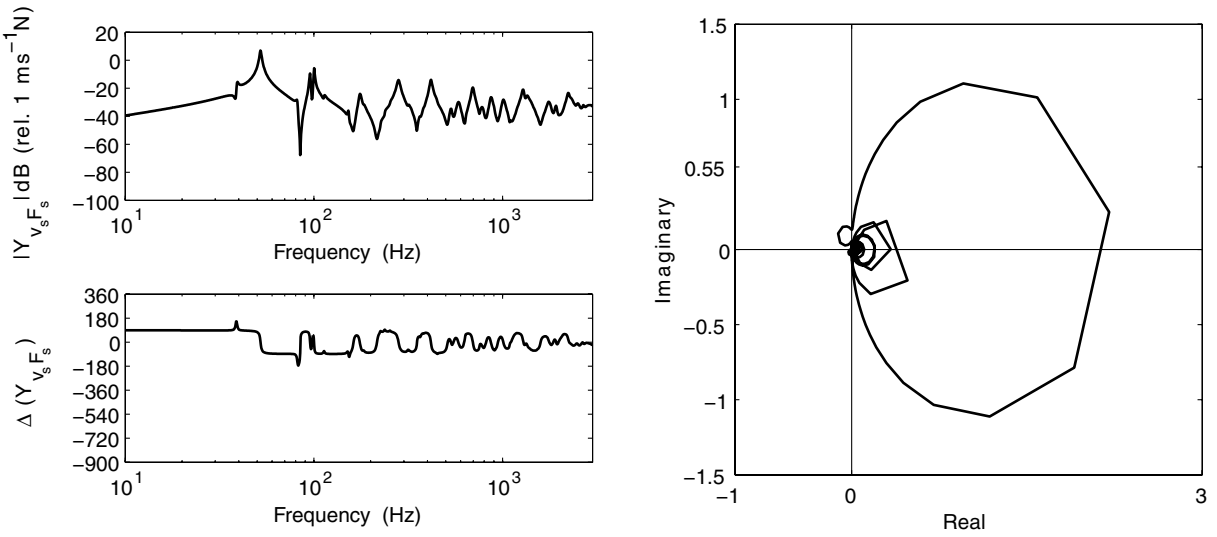

Fig. 12 Bode (left) and Nyquist (right) plots of the sensor-actuator FRF for the velocity weighting factor of $\alpha = 0$ with changed cavity boundary conditions.

instantaneously transmitted to the radiating panel, and vice versa, due to the cavity-air coupling path. The two transfer mobilities $T_{cc}^{s,r}(\omega)$ and $T_{cc}^{r,s}(\omega)$ have high amplitudes, primarily because of this strong air coupling.

The modeling problem presented in Sec. II of this paper assumes rigid side boundaries of the air cavity. Therefore, the air cavity is effectively sealed and the air is unable to flow in or out of the cavity if squeezed by the two panels. It is thus possible that different boundary conditions for the side surfaces of the cavity could influence the strength of the acoustical coupling and, consequently, the critical-velocity weighting factor. The simulations presented next were performed using an open-sided-cavity model, which allows the movement of air in and out of the cavity. The remaining modeling features (such as materials, geometry, boundary conditions, etc.) of the double panel are the same as in case of the model problem described in Sec. II. Figure 12 shows Bode and Nyquist plots of the sensor-actuator open-loop FRF, using a reactive actuator located in the center of the panel and using only one collocated sensor at the radiating-panel junction of the actuator. This corresponds to the use of the velocity weighting factor equal to zero.

It can be seen that in this case, the negative real part of the FRF is negligible in comparison with the closed-cavity case FRF, shown in Fig. 7b. Although the FRF is not exactly minimum-phase, there are no 180-deg phase lags. This is due to the weakened acoustical coupling path, because the cavity air is now free to flow in and out of the cavity so that the two plates can perform relatively independent motion. Figure 13 shows the value of the FRF maximal negative real part δ_0 plotted against the velocity weighting factor α.

The plot shows that the range of the weighting factors that result in unconditional stability is now extended, and zero weighting factors can offer a large enough margin to apply considerable feedback gains. In practice, this means that only one sensor located at the radiating plate junction of the control actuator is needed.

In conclusion, it can be stated that the acoustical coupling path is of great importance with respect to the stability of the feedback loops. Theoretically, it can be weakened by imposing a vacuum in the cavity. In practice, it can be significantly weakened by opening the side boundaries of the cavity. In any case, unconditionally stable velocity feedback loops are achievable by choosing an appropriate velocity weighting factor that has to be determined for the particular double-panel system.

V. Conclusions

In this paper, a theoretical analysis is presented of a smart double-panel system with decentralized feedback vibration control. Active control is implemented using a 4×4 regular array of actuators

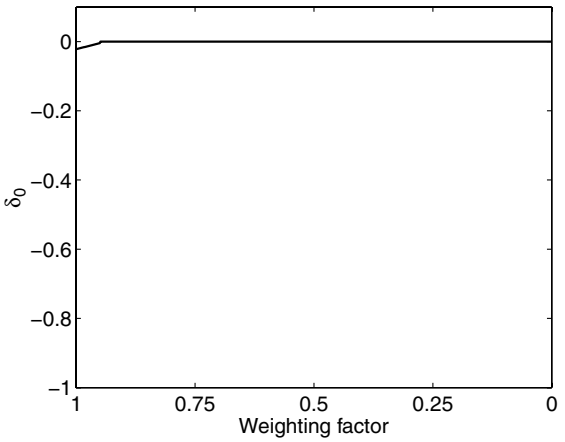

Fig. 13 The largest negative real part of the FRF, δ_0, plotted against the velocity weighting factor α when the four side surfaces of the air cavity are assumed open.

located in the air cavity, which can react from the two plates. The error signals are formed by a combination of two weighted velocities, which are measured by two sensors located at the actuator junctions on either plate. By using different velocity weighting factors, a variety of error signals can be created that determine the performance and the stability of the feedback loops.

Better broadband reductions of mean kinetic energy of the radiating panel and the sound-transmission ratio are obtained for weighting factors that emphasize the radiating-panel velocities. However, if only radiating-panel velocities are used for the error signal, only conditionally stable loops are possible. It is shown that this outcome is due to the acoustical and structural coupling of the two panels, which cause indirect-actuation paths. These indirect-actuation paths are particularly important at lower frequencies. It was shown that the main indirect-actuation effect is caused by the air cavity (acoustical path), whereas the elastic-mount system (structural path) is of minor importance.

Stable feedback control loops and a good performance can be obtained when source and radiating-panel error velocities are weighted by the critical value of the weighting factor in which the feedback loops change from unconditional stability to conditional stability. It was noted that the critical weighting factor α_{crit} depends upon the location of the control unit. Units close to the boundaries of the plates have critical α values as low as zero.

A sensitivity study demonstrated that the stiffness of the source panel influences the gain margin of the conditionally stable loops and

the critical α value. The critical value decreased to zero by increasing the stiffness of the source panels. However, unrealistically stiff source panels are needed to achieve unconditional stability with one sensor per actuator.

The critical value of the velocity weighting factor is also sensitive to the acoustical coupling strength. The acoustical coupling was addressed via the air density in the cavity. However, high vacuum is needed to reduce the critical α toward zero. But if open side boundaries of the air cavity are used instead of closed side boundaries, the zero frequency mode of the air in the cavity no longer exists and only one sensor per reactive actuator is needed for unconditionally stable loops; that is, α_{crit} is equal to zero.

Acknowledgments

The theoretical work presented in this paper was performed by Neven Alujević within the European Doctorate in Sound and Vibration Studies (EDSVS), which is supported by the European Commission through the Marie Curie Early-Stage Training Fellowships.

References

[1] Mixson, J. S., and Wilby, J. S., "Interior Noise," *Aeroacoustics of Flight Vehicles, Theory and Practice*, edited by Hubbard, H. H., NASA Langley Research Center, Hampton, VA, 1995, pp. 271–335.

[2] Fahy, F. J., and Gardonio, P., *Sound and Structural Vibration*, Elsevier, London, 2006.

[3] Fahy, F. J., *Engineering Acoustics*, Academic Press, London, 2001.

[4] Gardonio, P., and Elliott, S. J., "Active Control of Structure-Borne and Airborne Sound Transmission Through Double Panel," *Journal of Aircraft*, Vol. 36, No. 6, Nov.–Dec. 1999, pp. 1023–1032.

[5] Maury, C., Gardonio, P., and Elliott, S. J., "Model for Active Control of Flow-Induced Noise Transmitted Through Double Partitions," *AIAA Journal*, Vol. 40, No. 6, June 2002, pp. 1113–1121.

[6] Carneal, J. P., and Fuller, C. R., "Active Structural Acoustic Control of Noise Transmission Through Double Panel Systems," *AIAA Journal*, Vol. 33, No. 4, Apr. 1995, pp. 618–623.

[7] Elliott, S. J., Gardonio, P., Sors, T. C., and Brennan, M. J., "Active Vibroacoustic Control with Multiple Local Feedback Loops," *Journal of the Acoustical Society of America*, Vol. 111, No. 2, 2002, pp. 908–915.
doi:10.1121/1.1433810

[8] Preumont, A., *Vibration Control of Active Structures*, Kluwer Academic, London, 2002.

[9] Clark, R. L., Saunders, W. R., and Gibbs, G. P., *Adaptive Structures*, 1st ed., Wiley, New York, 2002.

[10] Gardonio, P., "Review of Active Techniques for Aerospace Vibro-Acoustic Control," *Journal of Aircraft*, Vol. 39, No. 2, Mar.–Apr. 2002, pp. 206–214.

[11] Alujević, N., Gardonio, P., and Frampton, K. D., "Smart Double Panel with Decentralized Active Damping Units for the Control of Sound Transmission," *AIAA Journal* (to be published).

[12] Gardonio, P., "Sensor-Actuator Transducers for Smart Panels," *ACTIVE 2006* [CD-ROM], Australia Acoustical Society, Adelaide, Australia, 18–20 Sept. 2006.

[13] Balas, M. J., "Direct Velocity Control of Large Space Structures," *Journal of Guidance and Control*, Vol. 2, No. 3, 1979, pp. 252, 253.

[14] Sun, J. Q., "Some Observations on Physical Duality and Collocation of Structural Control Sensors and Actuators," *Journal of Sound and Vibration*, Vol. 194, No. 5, pp. 765–770.
doi:10.1006/jsvi.1996.0394, 1996.

[15] Jayachandran, V., and Sun, J. Q., "Unconditional Stability Domains of Structural Control Systems Using Dual Actuator-Sensor Pairs," *Journal of Sound and Vibration*, Vol. 208, No. 1, pp. 159–166.
doi:10.1006/jsvi.1997.1177., 1997.

[16] Gardonio, P., Bianchi, E., and Elliott, S. J., "Smart Panel with Multiple Decentralised Units for the Control of Sound Transmission, Part 1: Theoretical Predictions," *Journal of Sound and Vibration*, Vol. 274, Nos. 1–2, pp. 163–192, 2004.
doi:10.1016/j.jsv.2003.05.004

[17] Gardonio, P., Bianchi, E., and Elliott, S. J., "Smart Panel with Multiple Decentralised Units for the Control of Sound Transmission, Part 2: Design of the Decentralised Control Units," *Journal of Sound and Vibration*, Vol. 274, Nos. 1–2, pp. 193–213, 2004.
doi:10.1016/j.jsv.2003.05.007

[18] Gardonio, P., Bianchi, E., and Elliott, S. J., "Smart Panel with Multiple Decentralised Units for the Control of Sound Transmission, Part 3: Control System Implementation," *Journal of Sound and Vibration*, Vol. 274, Nos. 1–2, pp. 215–32, 2004.
doi:10.1016/j.jsv.2003.05.006

[19] Gardonio, P., Lee, Y. S., Elliott, S. J., and Debost, S., "Analysis and Measure of a Matched Volume Velocity Sensor and Uniform Force Actuator for Active Structural Acoustic Control," *Journal of the Acoustical Society of America*, Vol. 110, No. 6, Dec. 2001, pp. 3025–3031.
doi:10.1121/1.1412448

[20] Paulitsch, C., Gardonio, P., and Elliott, S. J., "Active Vibration Control Using an Inertial Actuator with Internal Damping," *Journal of the Acoustical Society of America*, Vol. 119, No. 4, Apr. 2006, pp. 2131–2140.
doi:10.1121/1.2141228

[21] Benassi, L., and Elliott, S. J., "Active Vibration Isolation Using an Inertial Actuator with Local Displacement Feedback Control," *Journal of Sound and Vibration*, Vol. 278, Nos. 4–5, 2004, pp. 705–724.
doi:10.1016/j.jsv.2003.10.065

[22] Elliott, S. J., Serrand, M., and Gardonio, P., "Feedback Stability Limits for Active Isolation Systems with Reactive and Inertial Actuators," *Journal of Vibration and Acoustics*, Vol. 123, No. 2, 2001, pp. 250–261.
doi:10.1115/1.1350822

[23] Alujević, N., Frampton, K. D., and Gardonio, P., "Smart Double Panel with Decentralised Active Dampers for Control of Sound Transmission," Inst. of Sound and Vibration Research, TM 972, Southampton, England, U.K., 2007.

[24] Meirovitch, L., *Dynamics and Control of Structures*, Wiley, New York, 1990.

J. Wei
Associate Editor